



Wear Behavior of P/M High Nb Containing γ -TiAl Alloy in Different Environments

Jingwen Qiu^{1,2} · Zhengfan Fu¹ · Bin Liu² · Yong Liu² · Jianhui Yan¹ · Di Pan² · Weidong Zhang³

Received: 21 February 2019 / Accepted: 21 April 2019 / Published online: 25 May 2019
© The Korean Institute of Metals and Materials 2019

Abstract

The wear behavior of Ti–45Al–7Nb–0.3W (at%) alloy prepared by powder metallurgy (P/M) has been investigated using pin-on-disk wear tests at the room temperature. The dry sliding wear tests were performed against on a zirconia disk in different environments, viz, argon, hydrogen in nitrogen mixture, air and oxygen. The worn surfaces of Ti–45Al–7Nb–0.3W pins and wear debris were examined by scanning electron microscope, X-ray diffractometer and X-ray photoelectron spectroscopy. It was found that the high Nb containing Ti–45Al–7Nb–0.3W alloy didn't exhibit better wear resistance in the presence of oxygen than commercial γ -TiAl (Ti–47Al–2Nb–2Cr–0.2W) alloy. The oxidation on the worn surface and spalling of oxides caused by the mechanical force during sliding were the main reason for the high wear losses in the air and oxygen. The zirconia disk underwent a phase transformation caused by the high contact temperature and stress during the sliding tests. The abrasive particles produced in the wear tests largely consisted of the zirconia particles in different environments, except in the pure oxygen. The hard zirconia debris was embedded into the friction layer on the worn surfaces of TiAl pins, which provided protection against wear to some extent. The main wear mechanisms of Ti–45Al–7Nb–0.3W alloy were abrasive wear of two-body and three-body, some delamination and plastic deformation.

Keywords Ti–Al–Nb alloy · Tribological properties · Wear and friction

1 Introduction

Since TiAl alloys exhibit many attractive properties, such as high specific strength, good oxidation resistance, and creep properties, they have become an outstanding candidate of high-temperature structural materials in the commercial aircraft engines, automotive and energy industry [1, 2]. Many references [3–5] indicate that Nb can work as a β -stabilizing alloying element for TiAl alloys and can help to improve the deformability of TiAl alloys at high temperatures. Moreover, TiAl alloys with the high addition of Nb offer excellent

oxidation resistance, as demonstrated for turbine wheels in turbocharger applications [6, 7]. As the 3rd generation TiAl alloys, high Nb containing TiAl alloys have drawn lots of attention [8]. The wear resistance is another challenge to the TiAl alloy when they work as moving parts in the aerospace and automotive industries [9]. Over the past years, the wear behaviors of the 2nd generation γ -TiAl alloys have been widely studied [10–13]. Some references [14, 15] have shown that TiAl alloys have poor wear resistance and are difficult to lubricate, which may hinder their application in tribological components. And the wear behaviors of γ -TiAl alloys are sensitive to the environments, especially in the oxygen-containing environment [16, 17]. It is well known that Nb replaces Ti^{4+} in TiO_2 with Nb^{5+} valence to suppress TiO_2 growth and promotes the oxidation of Al to form dense Al_2O_3 [18, 19]. Obviously, Nb is effective to improve the oxidation resistance of TiAl. However, the wear behavior of high Nb containing TiAl alloy in different environments has been rarely reported.

In this paper, the dry sliding tests of Ti–45Al–7Nb–0.3W (at%) (referred to as Ti45Al7Nb alloy) against a zirconia disk were performed in different environments. The wear

✉ Bin Liu
binliu@csu.edu.cn

¹ Hunan Provincial Key Laboratory of High Efficiency and Precision Machining of Difficult-to-Machine Material, Hunan University of Science and Technology, Xiangtan 411201, China

² State Key Laboratory of Powder Metallurgy, Central South University, Changsha 410083, Hunan, China

³ College of Materials Science and Engineering, Hunan University, Changsha 410083, Hunan, China

behaviors of high Nb containing γ -TiAl alloy in different environments are discussed.

2 Methods and Materials

The γ -TiAl alloy was prepared by hot isostatic pressing (HIPping) method at 1523 K for 5 h, using the nominal composition of Ti–45Al–7Nb–0.3W (at%) pre-alloy powder from the plasma rotating electrode process (PREP). As shown in Fig. 1 [20], a home-made device was employed to perform the pin-on-disk wear tests. The TiAl cylindrical wear pins were obtained from the HIPed ingot by a wire electrical discharge machine. The hemisphere tips of 9.5 mm diameter on the pins were fabricated by a lathe machine and polished to a mirror by sand papers (2000 mesh). The counterface disk was made of yttria-stabilized (2.8 mol% yttria) tetragonal zirconia (YSZ) and was polished to a surface finish of $\sim 0.03 \mu\text{m}$. The physical properties of the YSZ disk and the Ti45Al7Nb pins used in the sliding tests are shown in Table 1. Data for the YSZ disk come from Saint-Gobain Advanced Ceramics Company [21], and other data were measured in the lab. The Poisson ratio of Ti45Al7Nb alloy is the theoretical value. Dry sliding tests were conducted in the air, oxygen, argon and 4% (vol%) hydrogen in nitrogen mixture ($\text{H}_2 + \text{N}_2$) separately. The humidity of air in the lab was around 45%, and the argon, hydrogen/nitrogen mixture and oxygen were below 5%. The sliding speed was 1 m/s and the total sliding distance of each test was 1 km. Wear tests were repeated three times in each environment at room temperature (25 °C).

The mass of the Ti45Al7Nb pins was measured by a precision electronic auto-balance before and after each test

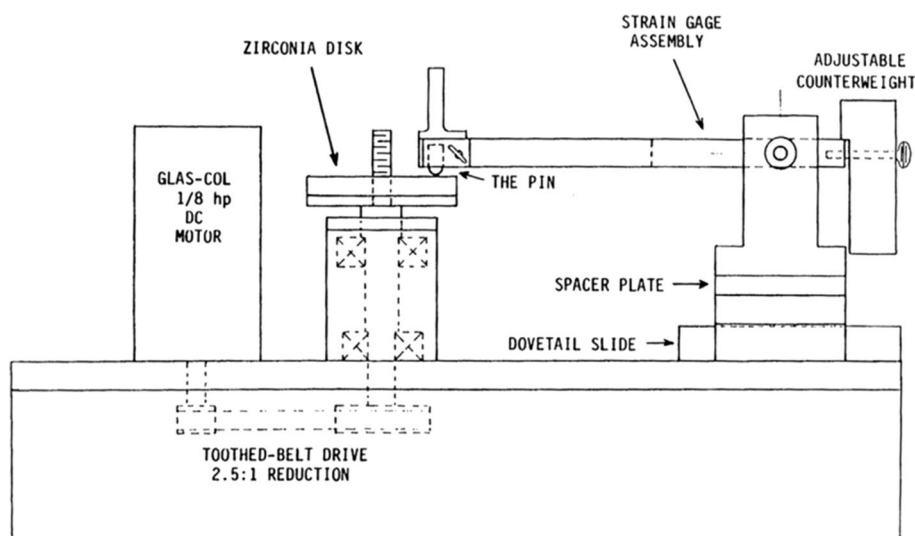
Table 1 Physical properties of YSZ disk and Ti45Al7Nb alloy

Material/property	ZrO ₂	Ti45Al7Nb
Hv, Hardness (GPa)	13.5	3.1
E, modulus of elasticity (GPa)	205	161
Density (kg/m ³)	6070	4234
Poisson's ratio	0.25	0.33
K, thermal conductivity (W/m K)	2.0	14.7
C, Specific heat (J/kg K)	630	–

to determine the wear loss. FEI XL-30 scanning electron microscope (SEM) equipped energy dispersive X-ray spectrometer (EDS) was used to investigate the wear particles and the worn tips of the TiAl pins. A Thermo Fisher X-ray photoelectron spectroscopy (XPS) system utilizing an Al K _{α} X-ray source (1486.6 eV) was used to analyze the elements on the worn surface of Ti45Al7Nb pins and the detecting depth was around 10 nm. High-resolution spectra of the Ti2p and Nb3d core level regions were recorded with the pass energy of 50 eV. Binding energies were corrected using the C1s peak of the residual carbon 284.8 eV to eliminate errors from the charging of the surface during measurement. A 3D optical surface profiler of Zygo Newview 7300™ was used to scan the wear tracks on YSZ disk.

The backscattered electron (BSE) image and energy dispersive X-ray spectrometer (EDS) of the as-HIPed Ti45Al7Nb alloy are presented in Fig. 2. As shown in Fig. 2a, the microstructure of Ti45Al7Nb alloy is mainly composed of γ phase (black) with a smaller amount of α_2 (gray) / γ lamellae phase. The α_2 phase is also distributed along the grain boundary of the γ phase.

Fig. 1 Schematic illustration of home-made wear tests device



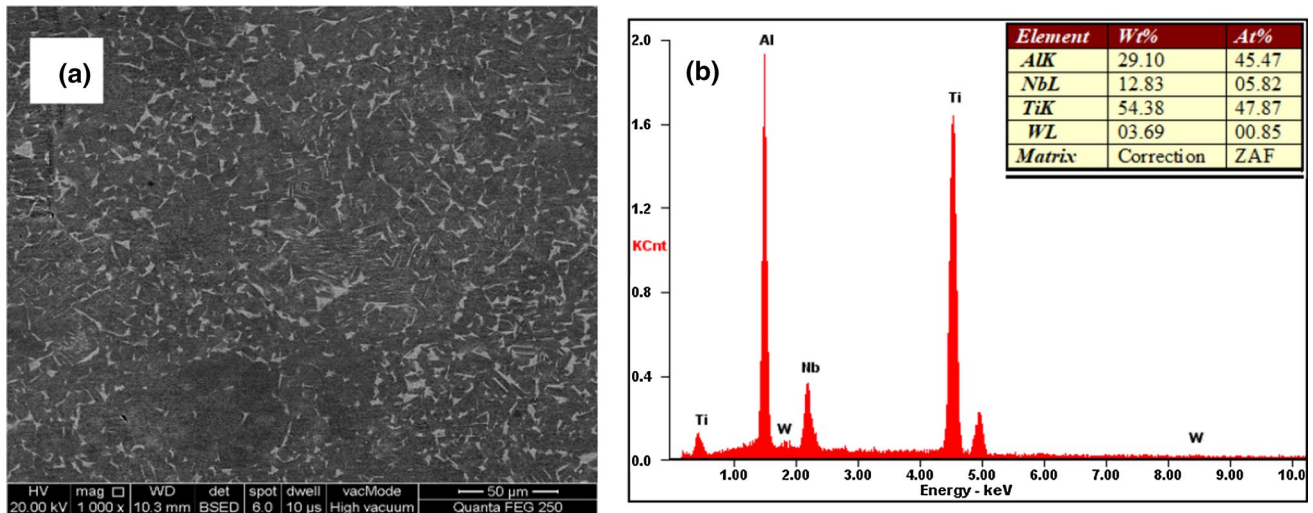


Fig. 2 a BSE image and b EDS spectra of the as-HIPed Ti45Al7Nb alloy

3 Results

3.1 Coefficients of Friction (COFs) and Wear losses

Figure 3a, b are typical curves of COFs versus time of Ti45Al7Nb and Ti-47Al-2Nb-2Cr-0.2W (alloy 4722) during sliding tests in different environments. The data of COFs versus time of alloy 4722 is from Ref. [16] in the same wear condition for comparison. For both γ -TiAl alloys, it is found that COFs in the non-oxygen environments were somewhat variable and the COFs in the oxygen-containing environments are relatively steady. The COFs of Ti45Al7Nb in the argon and hydrogen decreased from a higher initial value to a lower steady-state value. The COFs in the oxygen-free environments are higher than those in the oxygen-containing environments with the COF in oxygen showing the lowest value. References [12, 22, 23] indicated the TiO_{2-x} formed during sliding tests in the air and oxygen showed lubrication action, which contributed to the lower COFs in the oxygen-containing environments. Obviously, more TiO_{2-x} formed in the pure oxygen resulted in the lowest COF for both γ -TiAl alloys. The high Nb content in the TiAl seemingly displaces little difference in the COFs.

The mean wear loss and average COFs of Ti45Al7Nb and alloy 4722 in different environments are shown in Fig. 4a, b. The standard deviations were taken from three times wear tests in each environment. Note the data in Fig. 4b also come from the Ref. [16] in the same wear condition. The wear losses of both γ -TiAl alloys in the oxygen-containing environments are much more than those in the oxygen-free environments. The microhardness of alloy 4722 is 2.71 GPa [16], which is a little lower than that (3.10 GPa) of the Ti45Al7Nb in Table 1. According to the Archard wear equation, Ti45Al7Nb with higher hardness is supposed to

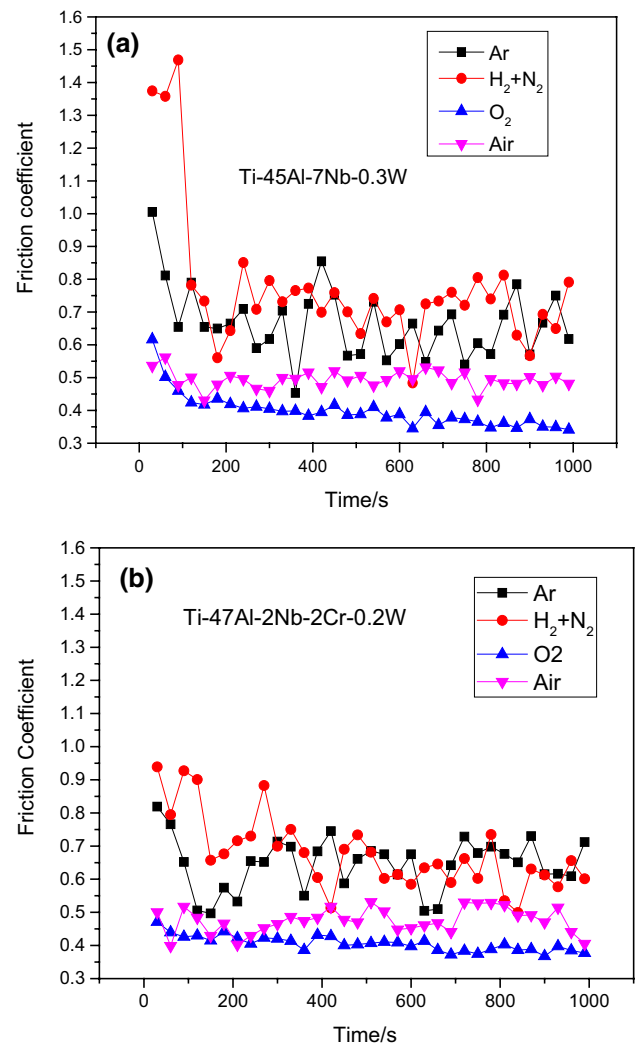


Fig. 3 Typical curves of COF versus time of a Ti45Al7Nb alloy and b alloy 4722 in different environments

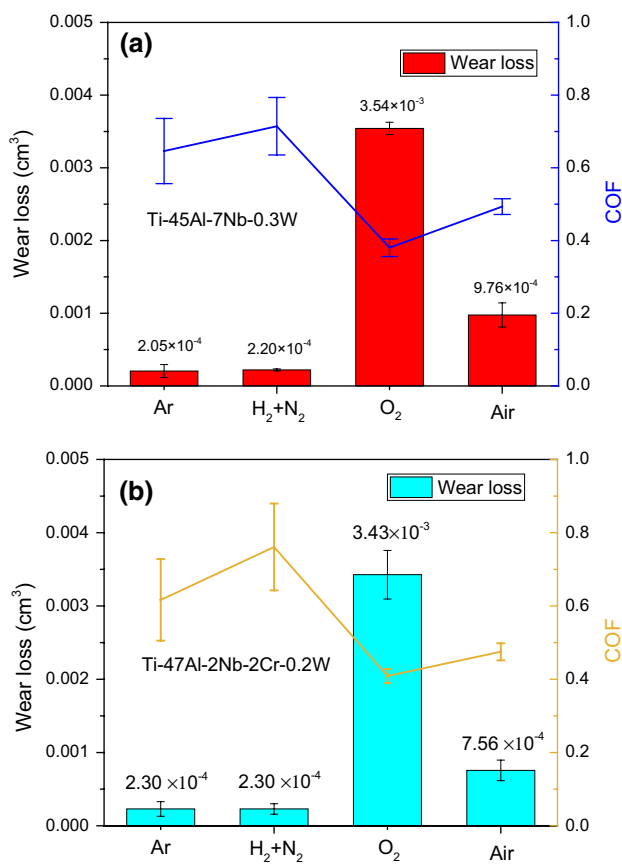


Fig. 4 Mean wear losses with COFs of **a** Ti45Al7Nb alloy and **b** alloy 4722 from three times repetitive wear tests in each environment

have better wear-resistance. On the other side, some studies [6, 18] have reported that high Nb content of TiAl-based alloys exhibit better oxidation resistance at high temperatures. The main reason is the Ti^{4+} in TiO_2 is substituted of by Nb^{5+} , which reduces the oxygen vacancy concentration and decreases the inward diffusion of oxygen. Meanwhile the addition of Nb promotes the oxidation of Al to form dense Al_2O_3 . Interestingly, Ti45Al7Nb did not exhibit distinguished wear-resistance, especially in the oxygen and air.

3.2 Debris

Figure 5a is X-ray diffraction (XRD) patterns from the debris collected from the wear tests performed in different environments. The wear debris produced in the argon is too little to be analyzed. The positions of possible cubic zirconia diffraction peaks have been indexed. It can be found the wear debris mainly consisted of cubic zirconia and a bit of TiAl, except in the pure oxygen. The debris in the oxygen was amorphous or nanocrystalline TiAl as indicated by the wide X-ray peak around 39° , which may arise from the highly localized stresses and the high contact temperature from friction heating (see Sect. 3.6). The peaks from cubic

zirconia debris confirm that the YSZ disk underwent a phase transformation from tetragonal phase to cubic phase during sliding tests.

The morphologies of wear debris and corresponding EDS spectra from the squares are shown in Fig. 5b–e, respectively. The wear debris produced in different environments is mainly irregular with some thin and flat pieces that may come from adhesive wear. More thin and flat particles were observed in the oxygen and air than in the argon and hydrogen. The EDS spectrum in Fig. 5c demonstrates the wear debris of Ti45Al7Nb alloy tested in the oxygen consisted of Ti and Al, with a little Zr and O elements. While, the EDS spectrum Fig. 5d indicates the wear debris in the argon consisted of Zr and O, with a little Ti and Al elements. Based on the XRD results in Fig. 5a, it can be found that the wear debris produced in argon, hydrogen and air were mainly zirconia, while the wear debris in the oxygen is mainly TiAl alloy debris. This indicates that the wear behavior of Ti45Al7Nb alloy was affected by the oxygen seriously, which is consistent with the wear losses shown in Fig. 4a.

3.3 Worn Surface

The morphologies with ESD results of worn surfaces on TiAl pins after sliding in different environments are exhibited in Fig. 6a–f. The area of the worn surface after sliding in the oxygen is the largest, see Fig. 6b. The long parallel plowing grooves and the wear pits marked in Fig. 6b are the characteristics of abrasive wear. BSE images shown in Fig. 6d, f indicate that there are amounts of foreign materials (bright areas) attached on the worn surfaces. The EDS spectrum in Fig. 6e demonstrates the large amount of white foreign materials should be the zirconia from the counterface. However, there was nearly no zirconia on the worn surface from tests in the pure oxygen, as shown in Fig. 6b, c. The micro-cracks on the worn surface in Fig. 6d may flake off by mechanical force during sliding and produce the wear debris. Some of the wear particles are adhered to the worn surface, which is also consistent with two-body and three-body abrasive wear processes.

Obviously, the oxygen plays a great role in the wear behavior of Ti45Al7Nb. XPS system was also employed to analyze the status of elements on the original surfaces of TiAl pin and the worn surfaces after sliding in the air and oxygen. The spectra of the $Ti2p$ and $Nb3d$ were compared, see Fig. 7a, b. The $Ti2p_{3/2}$ and $2p_{1/2}$ peaks corresponding to TiO_2 , and the $Nb3d_{3/2}$ and $3d_{5/2}$ peaks corresponding to Nb_2O_5 are present on the original surface at room temperature. It means that the original surface had been oxidized before the wear tests. The $Ti2p$ peaks corresponding to TiO_2 were also present on TiAl alloy after the wear tests in the air. The peak of $Ti2p$ (453.2 eV) occurred with $Ti2p_{3/2}$ and $2p_{1/2}$ together only after testing in oxygen, see Fig. 7a. The

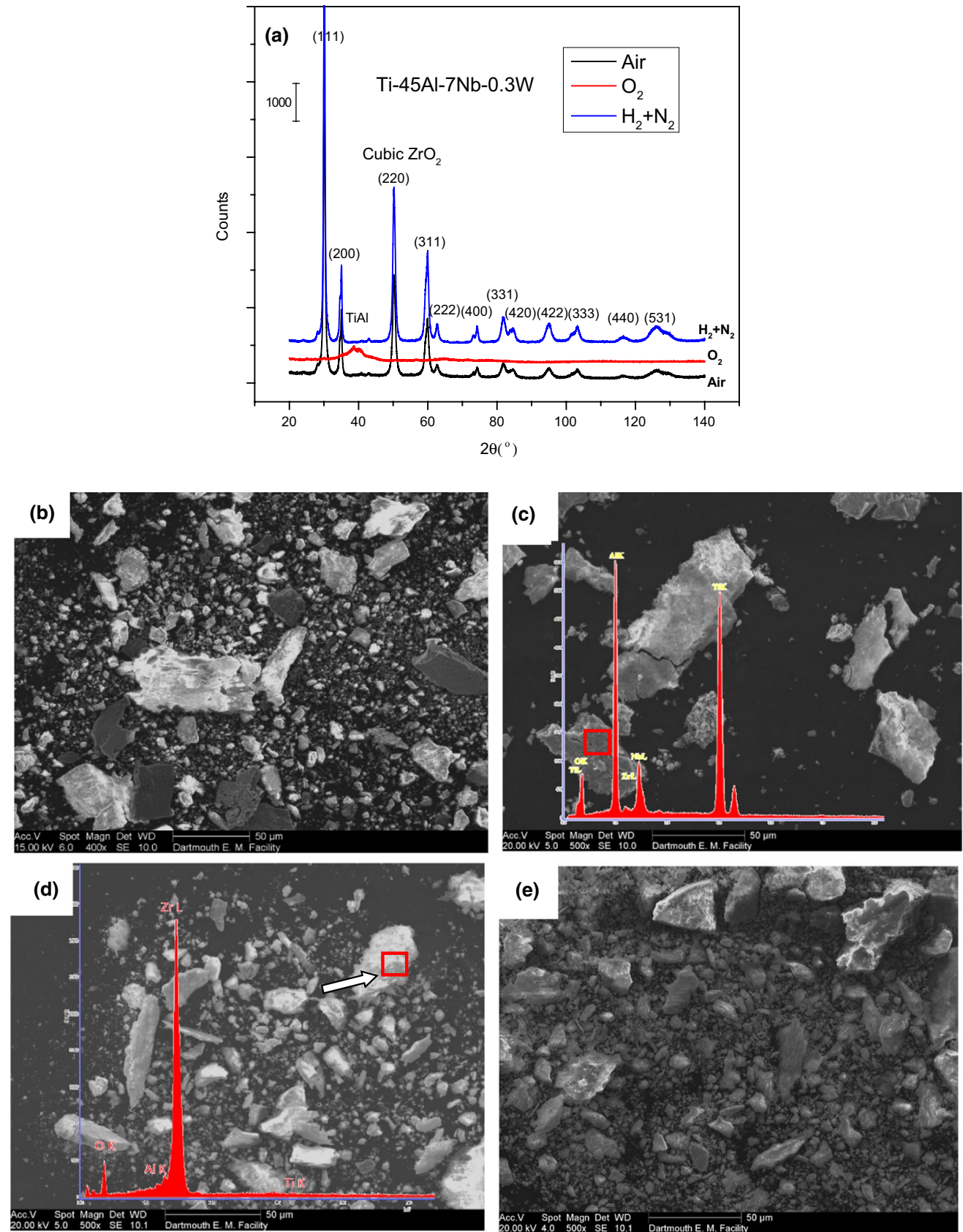


Fig. 5 a XRD patterns of debris collected during dry sliding tests and SE images with EDS spectra of debris produced in different environments: b air, c oxygen, d argon and e hydrogen

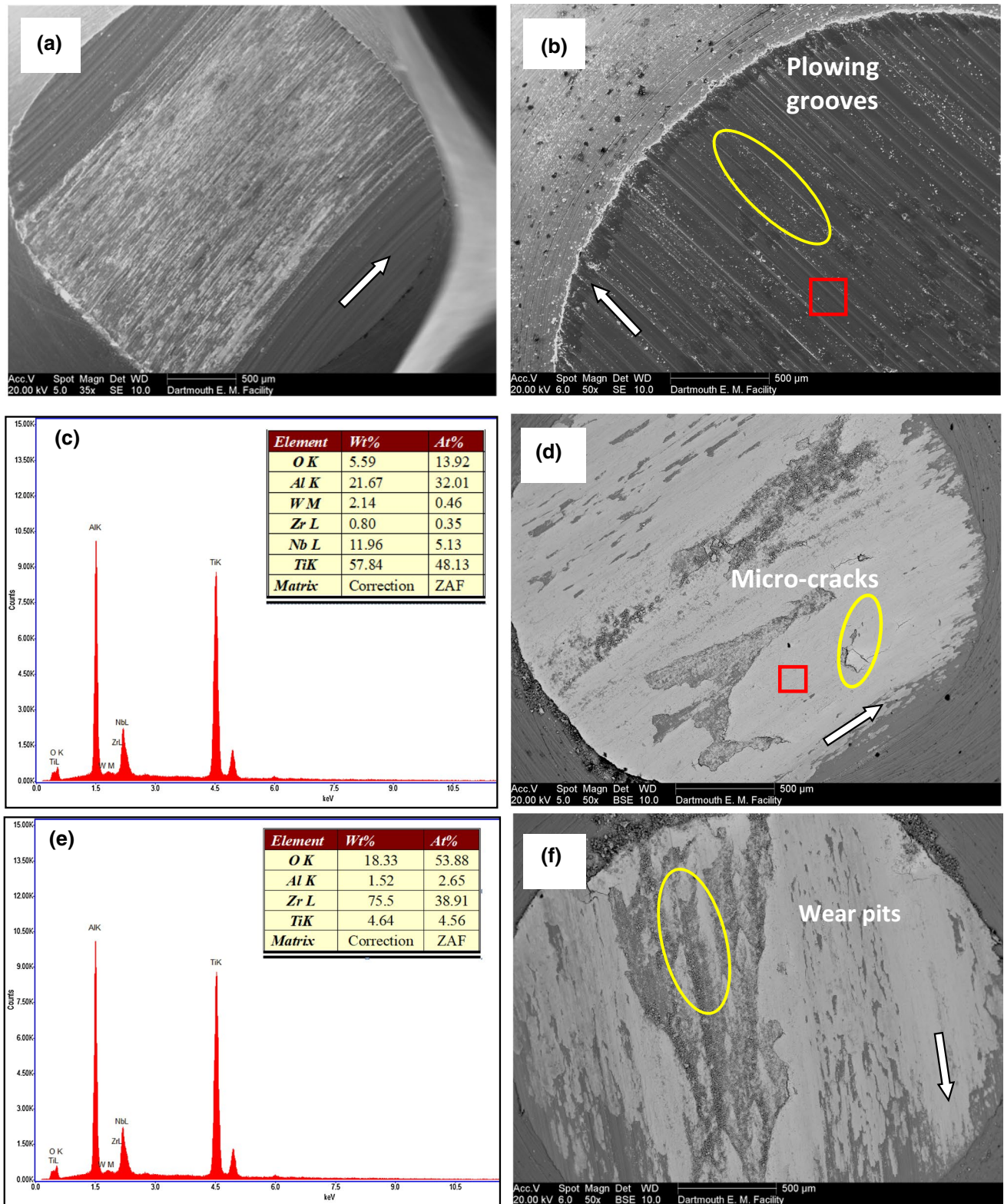


Fig. 6 SE and BSE images of worn surfaces and corresponding EDS spectra marked by the square: Ti45Al7Nb pins in **a**, **b**, **c** oxygen, **d**, **e** argon and **f** hydrogen. The direction of dry sliding is indicated by the arrow

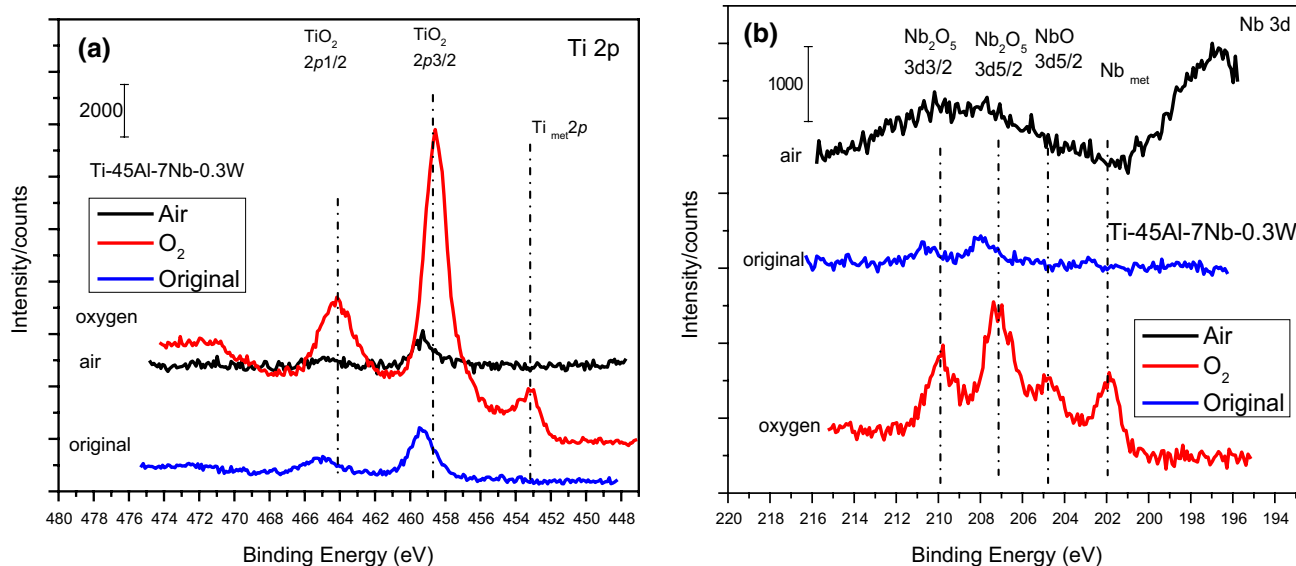


Fig. 7 XPS spectra of the worn surface and the original surface on Ti45Al7Nb pins **a** Ti2p and **b** Nb3d

Ti_{met}2p spectra likely come from the TiAl matrix. Similarly, the Nb_{met} spectra from the TiAl matrix were also present after testing in oxygen, see Fig. 7b. Since the detecting depth of the XPS system was around 10 nm and the thick zirconia would block the detecting from XPS, Ti_{met}2p and Nb_{met} spectra of the worn tip produced in the oxygen confirm little zirconia was attached on the Ti45Al7Nb pins. The result is consistent with the worn surface after sliding in the oxygen, as shown in Fig. 6b, c. The wide spectra of Nb3d may be several convoluted peaks. Based on peak fitting, it can be found that both Nb₂O₅ and NbO are present.

3.4 Zirconia Counterface

Since the counterface disk is too big to be observed in the scanning electron microscope, a 3D surface profiler were used to analyze the wear tracks on the YSZ disk, are shown in Fig. 8. Profile curves across wear tracks on YSZ disk are shown in Fig. 8a. It is evident that TiAl pins left obvious wear track on the YSZ disk after sliding in different environments, except in the pure oxygen. 3D image of wear track on YSZ disk produced in the oxygen displays more details in Fig. 8b, which demonstrates YSZ disk was hardly worn after sliding tests in the oxygen and some transferred materials which may come from TiAl pins were attached to the surface. It is a typical feature of adhesive wear. The 3D image in Fig. 8c shows the deepest wear track produced in the hydrogen. In the Table 1, the YSZ shows much higher hardness than Ti45Al7Nb alloy. It is supposed that Ti45Al7Nb alloy is hard to bring in excessive wear on the YSZ disk. However, the zirconia attached on the worn tips of TiAl pins, see Fig. 6a, d, f, acted as hard material to make

the YSZ disk be worn seriously. Without the help of zirconia embedded in the worn surface, as shown in Fig. 6b, the Ti45Al7Nb pins didn't bring in excessive wear on the YSZ disk in the pure oxygen. Ma et al. [24] reported that a certain amount of hydrogen improves the compressive properties of Ti–44Al–6Nb (at%) alloy because of the hydrogen-induced solution strengthening and hydrogen-promoted dislocation motion. It may explain why TiAl pins produced the deepest wear track on the counterface in the hydrogen in Fig. 8a, c.

3.5 Cross-Section of the Worn Surface and Friction Layer

The friction layer plays an important role in the wear behavior. The cross-sectional morphologies with elemental distributions of TiAl worn surface after sliding tests in the argon and oxygen are shown in Fig. 9. The bright material adhered on the worn tip of Ti45Al7Nb pin after testing in argon was found in Fig. 9a. Figure 9c indicates that the bright material mainly consists of zirconium, which is consistent with Fig. 6d, e. The micro-cracks marked by the arrow in the friction layer may result in the zirconia on the worn surface was peeled off easily during sliding tests and bring in abrasive wear. As shown in Fig. 9e, no zirconia was attached on the worn surface of TiAl pin after test in oxygen, which is consistent with the results of Fig. 6b, c. And the plastic deformation along the sliding direction is evident in Fig. 9e. The distributions of titanium shown in Fig. 9b, f are homogeneous in the friction layer and TiAl matrix after wear tests in the argon and oxygen. As shown in Fig. 9g, the oxygen enrichment zone exists on the worn surface and little oxygen is observed in the TiAl matrix. There is

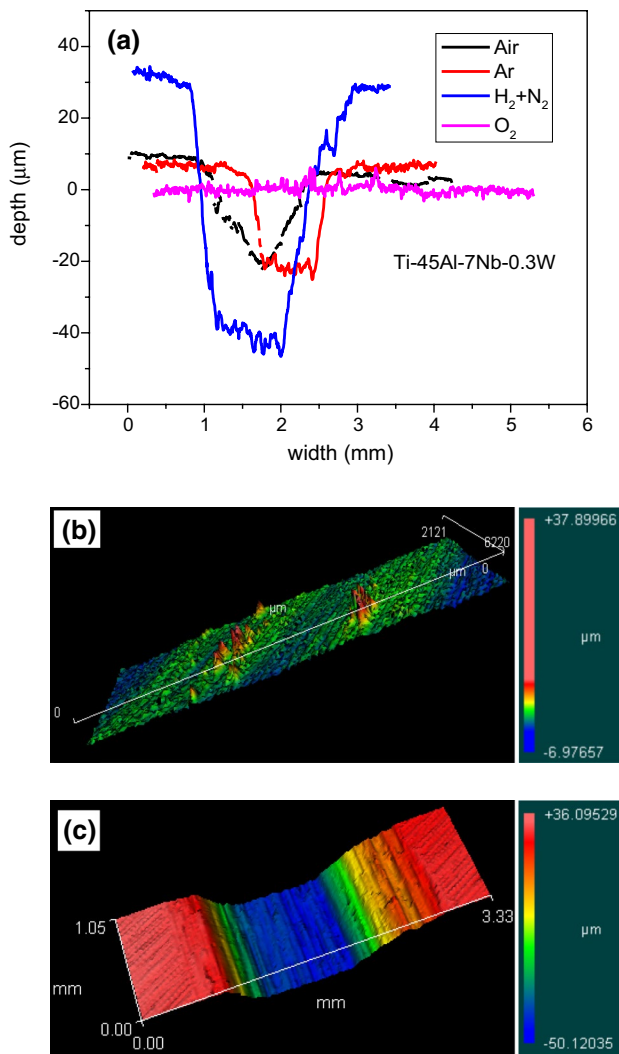


Fig. 8 **a** Profilometer traces across wear tracks on YSZ disk in different environments and 3D wear tracks on YSZ disk after wear test in **b** oxygen and **c** hydrogen

no difference about the distribution of Nb after sliding in the argon and oxygen, see Fig. 9d, h.

3.6 Estimate of Contact Temperature

It is well known that the contact temperature between the pin on disk has a close relationship with the oxidation [25, 26]. The methodology of Kennedy et al. [27] was employed to calculate the contact temperature rises. Here some important parameters and equations for the calculations are listed below. The total energy consumption rate during sliding tests is determined by the frictional force and the relative sliding speed. The rate of heat generated per unit area, q_{total} is given by

$$q_{total} = \frac{\mu \times w}{\pi a^2} \times V = q_p + q_d \quad (1)$$

where μ is the COF, a is the radius of contact circle between pin and disk, w is the load force, V is the sliding velocity, q_p is the generated heat enters into the contacting surface of the pin, q_d is the generated heat enters into the surface of the disk.

Kennedy et al. [27] defined the heat partitioning function, α , can be calculated from:

$$\alpha = \frac{q_p}{q_d} = \frac{\frac{1}{14.23\sqrt{V}} \left(\frac{a}{r_0^2} \right) + \frac{2.32}{k_d \sqrt{\pi(1.234+Pe)}}}{\frac{1}{k_p} \left(\frac{4a l_p}{d^2} + \frac{3\pi}{8} \right)} \quad (2)$$

where r_0 is the radius of the disk, K_d and K_p are the thermal conductivities of the YSZ disk and Ti45Al7Nb separately, Pe is the Peclet number ($Pe = va/2K_d$), l_p is the length of the pin and d is the diameter of the pin.

Then,

$$q_p = \left(\frac{\alpha}{\alpha + 1} \right) q_{total} = \left(\frac{\mu \times w \times V}{\pi a^2} \right) \left(\frac{\alpha}{\alpha + 1} \right) \quad (3)$$

The maximum contact temperature, T_{max} , can be calculated from:

$$T_{max} = T_{amb} + q_p \left[\frac{1}{14.23\sqrt{V}} \left(\frac{a^2}{r_0^2} \right) + \frac{2.32a}{k_d \sqrt{\pi(1.234 + Pe)}} \right] \quad (4)$$

where T_{amb} is the temperature of the ambient environment (25 °C). Note the radius (a) of the contact area between the TiAl pin and disk will become larger due to the abrasion in the sliding test, the T_{max} will decrease with the time of wear tests. Therefore, the Eq. (4) provides the maximum calculation of contact temperatures at the beginning of pin-on-disk sliding tests. The maximum contact temperatures of the tips on TiAl pins are shown in Table 2.

4 Discussion

Given the above, high Nb-containing Ti45Al7Nb alloy does not show better wear resistance in the oxygen-containing environment. As shown in Table 2, the highest contact temperatures of wear tests in different environments are all above 1100 °C. These contact temperatures are high enough to bring in the significant oxidation of Ti45Al7Nb in the air and oxygen. Based on the results in Sect. 3.3, it is found that the mechanical force during the rubbing process can easily break the oxide layer on the worn surfaces of Ti45Al7Nb pins. As shown in Fig. 6b, no dense oxide layer acts as a protective layer to prevent the TiAl from the further oxidation. The oxidation and spalling of oxides occurred alternately and repeatedly on the worn surface. This may be the main

Fig. 9 Cross-sectional morphologies of worn surface after sliding **a** in the argon with **b–d** Ti, Zr, Nb elemental distribution maps and **e** in the oxygen with **f–h** Ti, O, Nb elemental distribution maps

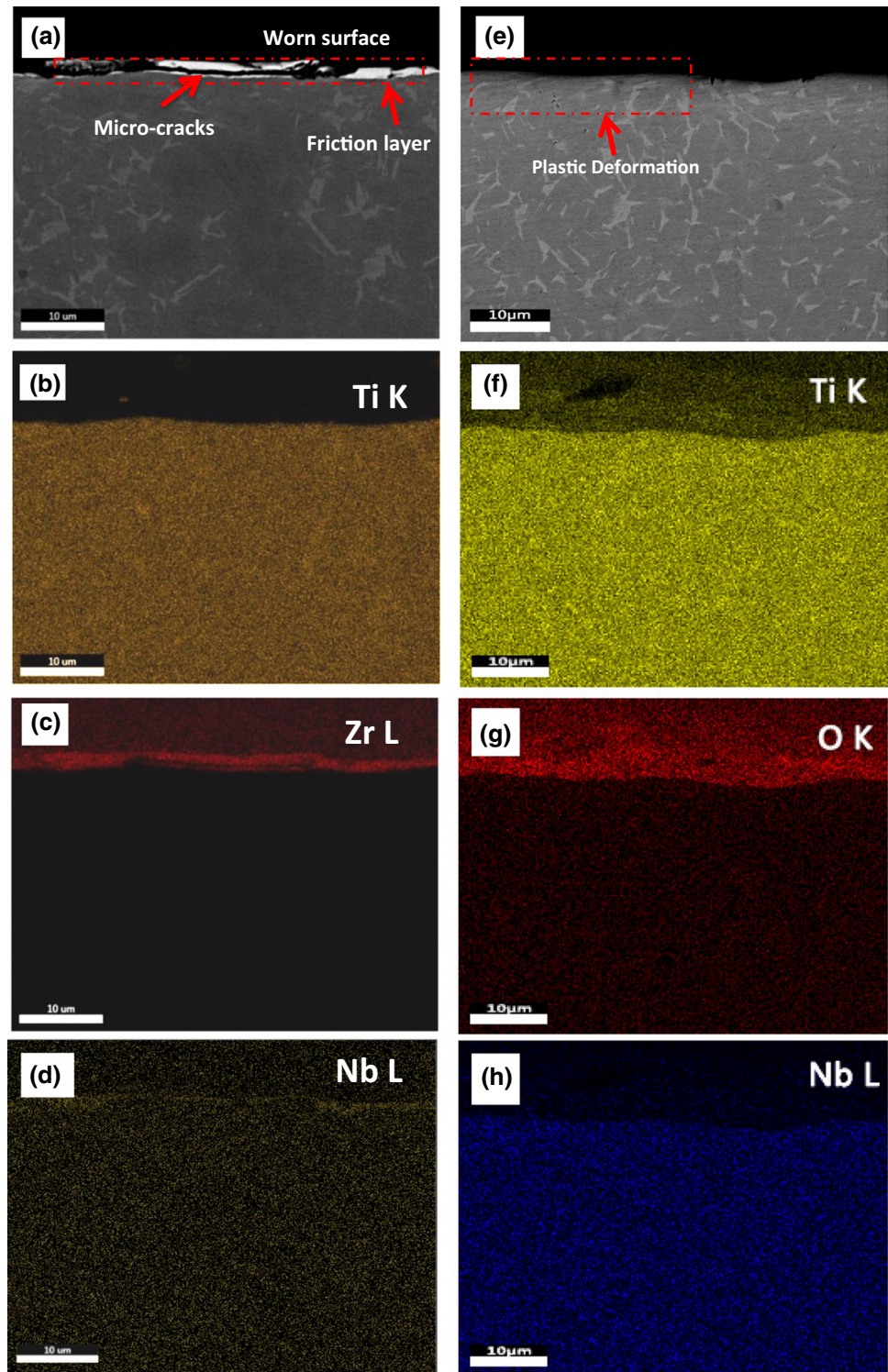


Table 2 Maximum contact temperatures (°C) of Ti45Al7Nb pins sliding on YSZ disk in different environments

Environments/alloys	Argon	Hydrogen/nitrogen	Oxygen	Air
Ti45Al7Nb	1992	2201	1183	1527

reason that Ti45Al7Nb alloy still had serious wear loss in the air and oxygen.

Chevalier et al. [28] indicated that YSZ with 2.8 mol% yttria will have a phase transformation from the cubic phase to the tetragonal phase at ~ 950 °C, which produces a volume change of the grain and micro-cracking on the worn surface

of the YSZ disk. The high contact temperature and localized stress would induce the phase transformation even in the tetragonal YSZ. The cubic zirconia indexed in the XRD patterns of the wear debris in Fig. 5a has confirmed that the YSZ disk underwent a phase transformation. With the help of repetitive shear stress, the YSZ disk would be abraded more and the zirconia particles removed from the YSZ disk could work as third-body abrasive particles to bring in more wear losses of YSZ disk and Ti45Al7Nb pins. Meanwhile the hard zirconia particles were embedded into the worn surface of Ti45Al7Nb pins to work as a protective layer which prevents the Ti45Al7Nb pins from being worn too much [16, 26, 29]. While, the lower contact temperatures during the wear tests in the oxygen, see Table 2, might be not high enough to induce the phase transformation on the YSZ disk. As shown in Fig. 6b, no zirconia debris was attached on the worn surface of Ti45Al7Nb alloy in the oxygen. And the amount of zirconia adhered on the worn surface in the air, see Fig. 6a, is also much less than those in Fig. 6d, f. No enough protection from the friction layer mixed with hard zirconia particles might be another reason why Ti45Al7Nb had such higher wear losses in the air and oxygen.

5 Conclusions

Dry sliding wear tests of Ti45Al7Nb alloy was performed on YSZ disk at 1 m/s for a 1 km sliding distance in different atmospheres. Based on the results above, the conclusions can be drawn as below:

The wear behaviors of high Nb containing Ti45Al7Nb alloy was sensitive to the oxygen but not to hydrogen. The high Nb content did not bring Ti45Al7Nb alloy better wear resistance in the oxygen-containing environments.

The friction layer mixed with hard zirconia particles on the Ti45Al7Nb pins provided protection against wear to some extent.

The main wear mechanisms of Ti45Al7Nb alloy are two-body and three-body abrasive wear, plastic deformation and delamination.

Acknowledgements The authors would like to thank Financial Supports of National Natural Science Foundation of China (51604112), Natural Science Foundation of Hunan Province of China (2017JJ3089), and National Natural Science Foundation of China (51774335). The authors thank Prof. Ian Baker at Dartmouth College, NH, US, for his assistance in the SEM and pin-on-disk wear tests device. The authors also thank Prof. Yu Wang at University of Science and Technology of China, for his useful suggestions. Prof. Yu Wang is supported by the Opening Project of State Key Laboratory of Explosion Science and Technology (KFJJ11-7M, Beijing Institute of Technology). The

zirconia disc was graciously provided by Dr. Oh-Hun Kwon of Saint-Gobain Research and Development Center, Northboro, MA, US.

References

1. B. Bewlay, M. Weimer, T. Kelly, A. Suzuki, P. Subramanian, *MRS Online Proc. Libr.* **1516**, 49 (2013)
2. R.E. Schafrik, *Metall. Mater. Trans. B* **47**, 1505 (2016)
3. B. Liu, Y. Liu, Y.P. Li, W. Zhang, A. Chiba, *Intermetallics* **19**, 1184 (2011)
4. Z.C. Liu, J.P. Lin, S.J. Li, G.L. Chen, *Intermetallics* **10**, 653 (2002)
5. H. Zhou, F. Kong, X. Wang, Y. Chen, *J. Alloys Compd.* **695**, 3495 (2017)
6. R. Pflumm, S. Friedle, M. Schütze, *Intermetallics* **56**, 1 (2015)
7. M. Naveed, A.F. Renteria, S. Weiß, *J. Alloys Compd.* **691**, 489 (2017)
8. H. Clemens, W. Smarsly, *Adv. Mater. Res.* **278**, 551 (2011)
9. M. Schütze, *JOM* **69**, 2602 (2017)
10. Z. Xu, L. Chen, X. Shi, Q. Zhang, A.M.M. Ibrahim, W. Zhai, J. Yao, Q. Zhu, Y. Xiao, *Tribol. Trans.* **58**, 668 (2015)
11. Z. Xu, X. Shi, Q. Zhang, W. Zhai, X. Li, J. Yao, S. Song, L. Chen, Y. Xiao, Q. Zhu, *Tribol. Trans.* **57**, 1017 (2014)
12. J. Cheng, J. Yang, X. Zhang, H. Zhong, J. Ma, F. Li, L. Fu, Q. Bi, J. Li, W. Liu, *Intermetallics* **31**, 120 (2012)
13. J. Cheng, S. Zhu, Y. Yu, J. Yang, W. Liu, *J. Mater. Sci. Technol.* **34**, 670 (2018)
14. C.X. Li, J. Xia, H. Dong, *Wear* **261**, 693 (2006)
15. A.R. Rastkar, A. Bloyce, T. Bell, *Wear* **240**, 19 (2000)
16. J. Qiu, Y. Liu, F. Meng, I. Baker, P. Munroe, *Intermetallics* **53**, 10 (2014)
17. J. Cheng, J. Ma, Y. Yu, L. Fu, Z. Qiao, J. Yang, J. Li, W. Liu, *J. Tribol.* **136**, 021604 (2014)
18. J. Lin, L. Zhao, G. Li, L. Zhang, X. Song, F. Ye, G. Chen, *Intermetallics* **19**, 131 (2011)
19. M. Yoshihara, Y.W. Kim, *Intermetallics* **13**, 952 (2005)
20. B.J. Johnson, F.E. Kennedy, I. Baker, *Wear* **192**, 241 (1996)
21. O.-H. Kwon, Saint-Gobain Advanced Ceramics, Northboro, MA, unpublished research (2012)
22. M.N. Gardos, H.-S. Hong, W.O. Winer, *Tribol. Trans.* **33**, 209 (1990)
23. M.N. Gardos, *Tribol. Trans.* **32**, 30 (1989)
24. T.F. Ma, R.R. Chen, D.S. Zheng, J.J. Guo, H.S. Ding, Y.Q. Su, H.Z. Fu, *Mater. Lett.* **213**, 170 (2018)
25. X. Wu, I. Baker, H. Wu, P.R. Munroe, *Intermetallics* **23**, 116 (2012)
26. Y. Lu, I. Baker, F.E. Kennedy, P.R. Munroe, *Intermetallics* **83**, 17 (2017)
27. F.E. Kennedy, Y. Lu, I. Baker, *Tribol. Int.* **82**(Part B), 534 (2015)
28. J. Chevalier, L. Gremillard, A.V. Virkar, D.R. Clarke, *J. Am. Ceram. Soc.* **92**, 1901 (2009)
29. J. Qiu, I. Baker, F.E. Kennedy, Y. Liu, P.R. Munroe, *Intermetallics* **40**, 19 (2013)

Publisher's Note Springer Nature remains neutral with regard to jurisdictional claims in published maps and institutional affiliations.